# Magnetoelectric Coupling through the Spin Flop Transition in $Ni_3TeO_6$

M. O. Yokosuk,[1] Amal al-Wahish,[1] Sergey Artyukhin,[2,3] K. R. O'Neal,[1] D. Mazumdar,[1] P. Chen,[1] Junjie Yang,[4]
Yoon Seok Oh,[2,5] Stephen A. McGill,[6] K. Haule,[2] Sang-Wook Cheong,[2,4,5] David Vanderbilt,[2] and J. L. Musfeldt[1,7]

[1]*Department of Chemistry, University of Tennessee, Knoxville, Tennessee 37996, USA*
[2]*Department of Physics and Astronomy, Rutgers University, Piscataway, New Jersey 08854, USA*
[3]*Quantum Materials Theory, Italian Institute of Technology, Via Morego 30, 16163 Genova, Italy*
[4]*Laboratory for Pohang Emergent Materials and Max Plank POSTECH Center for Complex Phase Materials,*
*Pohang University of Science and Technology, Pohang 790-784, Korea*
[5]*Rutgers Center for Emergent Materials, Rutgers University, Piscataway, New Jersey 08854, USA*
[6]*National High Magnetic Field Laboratory, Florida State University, Tallahassee, Florida 32310, USA*
[7]*Department of Physics and Astronomy, University of Tennessee, Knoxville, Tennessee 37996, USA*

We combined high field optical spectroscopy and first principles calculations to analyze the electronic structure of $Ni_3TeO_6$ across the 53 K and 9 T magnetic transitions, both of which are accompanied by large changes in electric polarization. The color properties are sensitive to magnetic order due to field-induced changes in the crystal field environment, with those around Ni1 and Ni2 most affected. These findings advance the understanding of magnetoelectric coupling in materials in which magnetic $3d$ centers coexist with nonmagnetic heavy chalcogenide cations.

Spin and polarization flop transitions are fascinating, especially when controlled by external stimuli like magnetic and electric fields and accompanied by large material responses involving multiple degrees of freedom [1–7]. Multiferroics like $MnWO_4$ and $TbMnO_3$ are flagship examples and owe their remarkable properties, including field control of polarization and polarization reversal accompanied by spin-helix reorientation, to the heavy ions that bring strong spin-orbit coupling and magnetic anisotropy [8–11]. $Ni_3TeO_6$ drew our attention due to the presence of both $3d$ and $5p$ cations, an unusual spin-flop transition [12–14], and a complex magnetic field-temperature phase diagram (Fig. 1). A magnetically induced electric polarization ($P = 3,280\ \mu C/m^2$) arises in the antiferromagnetic I (AFM I) phase below $T_N = 53$ K due to Heisenberg exchange striction in the polar structure, and a continuous spin-flop transition occurs at 9 T into the AFM II phase, altering the polarization ($\Delta P = 290\ \mu C/m^2$ at 2 K) [13]. Moreover, $Ni_3TeO_6$ sports the largest linear magnetoelectric coupling constant in a single-phase material known to date ($\alpha = 1,300$ ps/m) [13]. Metamagnetic transitions accompanied by extraordinarily large polarization changes have been discovered at 52 and 70 T [15], and indications of an unexplored transition between 30 and 35 T were observed as well [16]. The colossal polarization, rich magnetic phase diagram, and large spin-orbit coupling due to incorporation of the Te centers raise the possibility of large dynamic magnetoelectric coupling in this system.

In this Letter, we reach beyond static probes of magnetoelectric coupling in $Ni_3TeO_6$ to reveal the dynamic interactions between spin and charge sectors. In addition to interband transitions above 2 eV, we uncover a series of Ni $d$-to-$d$ excitations below 3 eV that are sensitive to magnetic order, evidence that spin-charge coupling persists to much higher energies than previously supposed. Moreover, by
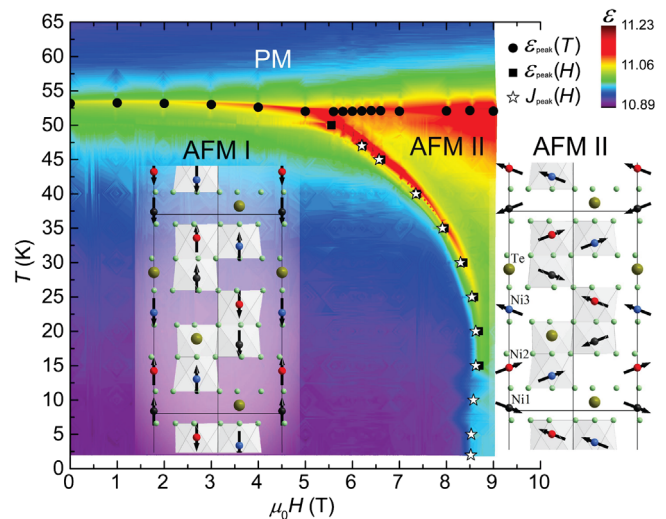


FIG. 1.   Phase diagram of $Ni_3TeO_6$ determined by variations in the dielectric constant $\epsilon$ (color scale at upper right) and magnetoelectric current. Closed circles, closed squares, and open asterisks indicate peak-center positions for $\epsilon(T)$, $\epsilon(H)$, and magnetoelectric current $J(H)$, respectively [13]. These peaks map the boundaries between the paramagnetic (PM) phase and antiferromagnetic phases (AFM I, AFM II). The structure of $Ni_3TeO_6$ is of the corundum type with a polar $R3$ space group, three inequivalent $S = 1$ Ni sites along $c$, and significant distortions of oxygen octahedra surrounding Ni ions [12]. The spin configurations in the AFM I and AFM II phases are shown schematically in the insets.

comparing field-induced changes in the color band excitations with predictions of Ni centers in specific crystal field environments, we determine how and why the crystal field environments—particularly around the Ni1 and N2 centers—respond to different microscopic spin arrangements. This technique of decomposing on-site excitations according to their precise local environment and analyzing the relative importance of different energy transfer processes can be applied to other materials in which transition metal and heavy chalcogenide cations coexist as well as those with complicated magnetic sublattices, thereby offering a site-specific perspective on electronic excitations in magnetic solids.

High quality single crystals were grown as described previously [13] and polished to thicknesses of $\approx 28$ $\mu$m. Optical transmittance was measured as a function of temperature in the $ab$ plane and along the $c$ direction using a series of spectrometers (0.4–3.0 eV; 4.2–300 K). Absorption was calculated as $\alpha(E) = -(1/d)\ln T(E)$, where $T(E)$ is the transmittance and $d$ is the sample thickness. Magneto-optical measurements were carried out at the National High Magnetic Field Laboratory in Tallahassee, Florida (4.2 K, 0–35 T). The first-principles calculations were performed using the Elk full-potential code using linearized augmented plane-wave basis [17], LDA + U in the fully localized limit [18] with Slater parameters $F^{(0)} = 8.0$ eV, $F^{(2)} = 8.18$ eV, $F^{(4)} = 5.11$ eV [19], and the Perdew-Wang/Ceperley-Alder exchange-correlation functional [20]. The 20-atom rhombohedral magnetic unit cell with the $\uparrow\uparrow\downarrow\downarrow\downarrow\uparrow$ magnetic ordering was used in the calculations, and a $4 \times 4 \times 4$ $k$-point grid was employed for reciprocal-space sampling.

Figure 2 displays the absorption of $Ni_3TeO_6$ in the $ab$ plane and $c$ direction at 300 and 4.2 K. We clearly observe two broad bands below 2 eV. Focusing first on the $ab$-plane data, we find color band excitations near 1.0, 1.55, and 1.72 eV. Each appears with significant oscillator strength due to noncentrosymmetric local environments around each of the Ni sites. Combined with the absorption minimum near 2.25 eV and small shoulder at 2.5 eV, these features are responsible for the striking green color of the crystal. The absorption rises sharply above 2.6 eV, suggesting the start of strong interband transitions. As shown in the Supplemental Material [21], there are no spectral changes across the Néel transition.

To test whether the lower-energy peaks might arise from interband transitions, we calculated the Kohn-Sham band structure at the LDA + U level for $Ni_3TeO_6$ in the zero-temperature antiferromagnetic configuration. The results are shown in Fig. 2, and where comparable, they are in excellent agreement with Ref. [14]. The gap, clearly visible in the density of states plot in Fig. 2(c), is determined to be 2.2 eV, which rules out any interband transitions below 2 eV. To drive this point home, the components of LDA + U optical dielectric response tensor calculated within the random phase approximation in the $q \to 0$ limit
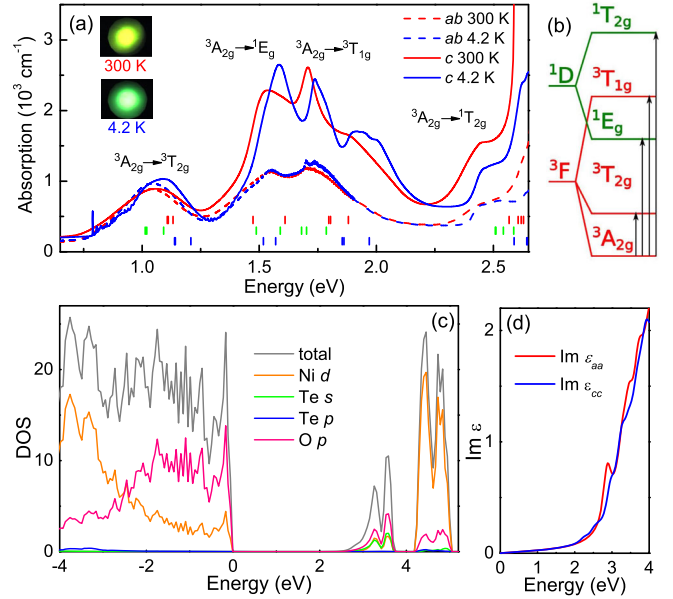


FIG. 2. (a) Absorption coefficient of $Ni_3TeO_6$, $\alpha(E)$, in the $ab$ plane and the $c$ direction at 300 and 4.2 K. Vertical lines near the bottom mark the computed $d$-to-$d$ excitations for the $d^8$ Ni ions, with red, green, and blue indicating excitations on Ni1, Ni2, and Ni3 sites, respectively. The insets show photographs of the crystal along $c$. (b) The splitting of free Ni ion $d^8$ multiplets in the presence of an octahedral crystal field excitations between these levels. (c) Ion-projected density of states per magnetic unit cell obtained from density functional theory (DFT) and (d) in-plane ($\varepsilon_{aa}$) and $c$-axis ($\varepsilon_{cc}$) components of the dielectric tensor calculated within the random phase approximation in the $q \to 0$ limit with no microscopic contributions.

are plotted in Fig. 2(d). The interband transitions naturally account for the sharply rising absorption near 2.6 eV [Fig. 2(a)]. They are dominated by excitations from hybridized O $p$ and majority Ni $e_g$ states at the top of the valence band to Te $s$ and minority Ni $e_g$ conduction bands. We therefore assign the features below 2 eV to on-site Ni $d$-to-$d$ excitations, an assignment that is strengthened by the resemblance to $Ni_3V_2O_8$ [5], where similar $d$-to-$d$ transitions occur and where the charge-transfer gap of 2.4 eV is only slightly smaller than ours. We shall give further theoretical support for this assignment shortly.

Returning to the experimental data and focusing now on comparing the $c$ axis response of $Ni_3TeO_6$ with the in-plane spectra [Fig. 2(a)], we immediately notice that while the intensities of the 1.2 eV peaks are similar, there is a large anisotropy between 1.5 and 2.2 eV, with the absorption being much stronger along $c$ ($\approx 2500$ cm$^{-1}$) than in the $ab$ plane ($\approx 1300$ cm$^{-1}$). Temperature effects are also more interesting in this direction, with the 4.2 K data showing (i) an overall hardening of the excitations, (ii) an intensity increase near 1.9 eV, and (iii) fine structure on the leading edge of the 1.1 eV band that may correspond to phonon side bands [16]. Examination of the 1.9 eV excitation reveals that the peak

shape is a strong function of temperature. The additional orange light absorption at 4.2 K causes $Ni_3TeO_6$ to appear more green to the naked eye [inset, Fig. 2(a)].

As noted above, we have assigned the color-band excitations below 2.5 eV to on-site $d$-to-$d$ transitions, which are not expected to appear in a single-particle framework such as DFT + U. To confirm this assignment, we turn to a crystal field model. The Coulomb interactions for a spherically symmetric $d^8$ ion give rise to the ground state $^3F$. These are correlated states that generally cannot be represented as a single Slater determinant. In particular, the state with the largest orbital moment, $2^+2^-$, where both holes in the $d$ shell have $m_l = 2$ and opposite spins (indicated by superscripts "+" and "−"), is a single Slater determinant. Instead, the state obtained by applying the angular momentum lowering operator $L^-$, and thus belonging to the same multiplet, is made up of the microstates $2^+1^-$ and $2^-1^+$, and so is not a single-determinant state [22,23]. The next multiplet is $^1D$, followed by $^3P$, $^1G$, and $^1S$ states. In the (approximately) octahedral crystal field of the oxygen cage surrounding the Ni ions, the lowest multiplet splits as $^3F \rightarrow \Gamma_2 = {^3A_{2g}}$ ($E = -12Dq$), $\Gamma_5 = {^3T_{2g}}$ ($E = -2Dq$), and $\Gamma_4 = {^3T_{1g}}$ ($E = 6Dq$), where $10Dq$ corresponds to the splitting of a single $d$ level that would be produced by the same octahedral crystal field. The next lowest multiplet splits as $^1D \rightarrow \Gamma_3 = {^1E_g}$ ($E = 5F_2 + 45F_4 - \frac{24}{7}Dq$) and $^1T_{2g}$ ($E = 5F_2 + 45F_4 + \frac{16}{7}Dq$). These splittings are shown schematically in Fig. 2(b), where the vertical black arrows indicate the optical excitations of interest.

In order to estimate the $d$-to-$d$ transition energies, we performed exact diagonalization of an atomic Hamiltonian in the $d^8$ sector for each of the three inequivalent Ni sites.

The Hamiltonian included the Hund's exchange energy, $J_H = 0.9$ eV, and the orbital energies in the crystal field, approximated by the energies of Wannier functions obtained from the DFT calculations for each of the three Ni ions. The vertical marks in Fig. 2(a) show that these predicted excitation energies coincide well with the peaks observed in our experiment. The excitations near 1.0, 1.55, 1.72, and above 2.5 eV are therefore associated with transitions to the $\Gamma_5, \Gamma_3, \Gamma_4,$ and $\Gamma_5$ multiplets, respectively. This confirms the interpretation of the absorption bands below 2 eV as resulting from $d$-to-$d$ transitions. The assignment also clarifies that the shoulder near 2.5 eV is related to on-site excitations and not yet the beginning of the interband transitions. This framework and the position of the spectral peaks allow us to estimate that $Dq$ and the Racah parameter $B$ are both (coincidentally) equal to 0.11 eV, consistent with expectations for a $Ni^{2+}$ complex [24].

We now turn to the optical response in applied field. Figures 3(a) and 3(b) summarize the magneto-optical properties of $Ni_3TeO_6$ in the $ab$ plane ($B\|c$) and in the $c$ direction ($B\perp c$) at 4.2 K. The data are displayed as a set of absorption difference spectra, $\Delta\alpha(E, B) = \alpha(E, B) - \alpha(E, B = 0)$, for selected fields ranging from 4 to 35 T. The zero-field linear absorption $\alpha(E)$ is also shown at the bottom of panel (a) for reference. In general, the contrast increases with field, although the peak near 1.4 eV (related to changes in $^3A_{2g} \rightarrow {^1E_g}$ excitations) is an exception.

Figure 3(b) brings together the full field absorption difference spectra, $\Delta\alpha(E,B) = \alpha(E,B=35\,\text{T}) - \alpha(E,B=0\,\text{T})$, with the theoretical locations of the three different sets of $d$-to-$d$ transitions indicated at the bottom as in Fig. 2(a). Comparison of these spectra with the predicted crystal-field
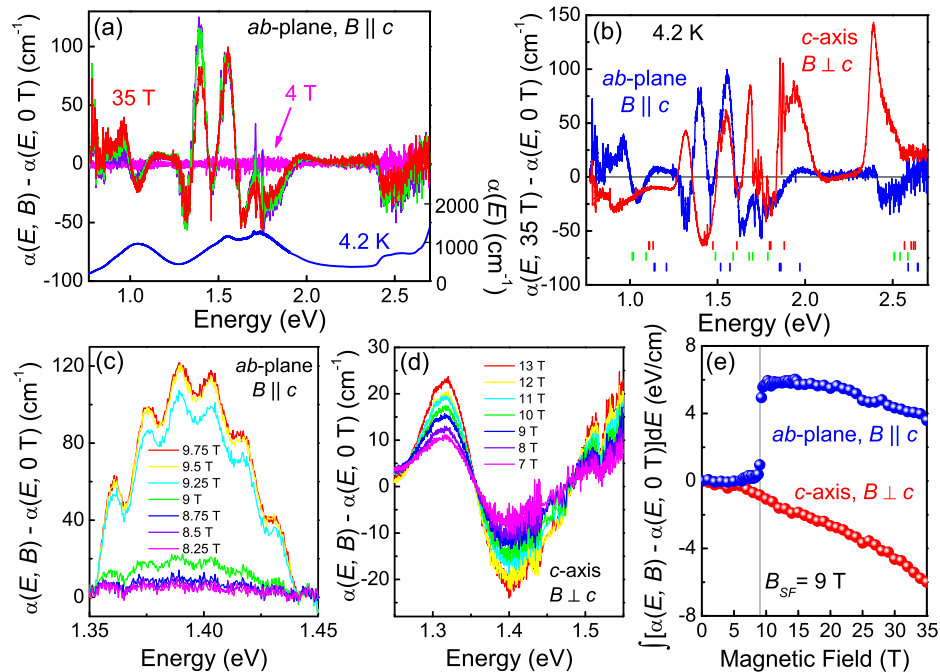


FIG. 3. Absorption difference spectra, $\Delta\alpha = [\alpha(E,B)\text{-}\alpha(E,B=0\,\text{T})]$, of $Ni_3TeO_6$ in the (a) $ab$ plane for $B\|c$ at selected fields up to 35 T: (pink 4 T, purple 10 T, green 20 T, red 35 T). The 4.2 K absolute absorption spectrum is included for comparison (on the bottom, in blue). (b) Full field (35 T) absorption difference spectra taken in the $ab$ plane and along the $c$ direction. Red, green, and blue vertical lines indicate the predicted $d$-to-$d$ excitations. (c,d) Absorption difference spectra in the $ab$ plane ($B\|c$) and $c$ direction ($B\perp c$) at selected fields around the spin-flop transition. (e) Integrated absorption difference of the data in panels (c) and (d).

excitations verifies that the observed features are due to field-induced changes in the Ni $d$-to-$d$ excitations.

Inspection of Fig. 3(c) reveals that the $ab$-plane absorption difference spectra ($B\|c$) display a sharp discontinuity across the 9 T spin flop transition. This discontinuity is not seen in the $c$-axis data of Fig. 3(d), which is not surprising since these were taken with $B\perp c$ where the spin-flop transition does not occur. Figure 3(e) quantifies these trends by plotting the absorption difference, integrated over an energy window near 1.4 eV, as a function of magnetic field. The $ab$-plane response to the magnetic field ($B\|c$) displays a sharp jump across the 9 T transition, along with precursor effects (both below and above the spin-flop transition) and no hysteresis (not shown). This indicates that the electronic properties are sensitive to changes in the microscopic spin pattern—a direct consequence of spin-charge coupling and analogous to the dielectric response in Fig. 1. By contrast, in the absence of a spin-flop transition, the $c$-axis response ($B\perp c$) shows only a gradual decrease in the integrated $\Delta\alpha$ with no distinguishing characteristics.

Another interesting aspect of the magneto-optical response is that $\Delta\alpha$ has not saturated by 35 T, suggesting that higher fields are likely to uncover new magnetic phases. Recent magnetization and magneto-infrared experiments do in fact reveal the possibility of an unexplored transition between 30 and 35 T as well as metamagnetic transitions at 52 and 70 T for $B\|c$ [15,16].

A close-up view of the color bands of $Ni_3TeO_6$ (Fig. 4) along with an analysis of the local structure [12,25] unveils the role of each of the three distinct Ni ions. The Ni3 centers, for instance, have a relatively irregular environment and strong crystal field associated with their face-shared proximity to the unusual $Te^{6+}$ cations (inset, Fig. 1).

As expected, this distorted environment correlates with the appearance of $d$-to-$d$ transitions (blue vertical lines) on the high-energy side of each cluster of predicted excitations. This is precisely the range with little or no magneto-optical response. By contrast, the Ni2 ions have the least distorted environment and weakest crystal field, and their predicted on-site excitations (green lines) are at lower energies compared to those of the other two Ni centers. Since absorption difference structures always appear on the leading edge of each band—both in the $ab$ plane and along $c$—we can conclude that Ni2 ions are involved. The same is true for the Ni1-related features, which are predicted to be in the middle. We therefore surmise that electronic structure changes through the spin flop transition derive from field-induced modifications to the crystal field environment of Ni1 and Ni2 (and associated adaptations in hybridization). Recent calculations support the dominant contribution of Ni1···Ni2 interactions to the magnetic properties [14] and magnetically induced electric polarization [15].

In summary, we bring together optical spectroscopy and first principles calculations to reveal how and why the electronic properties of $Ni_3TeO_6$ can be controlled by magnetic field, and we trace the color property tunability to field-induced changes in crystal field environments of the associated Ni $d$-to-$d$ excitations. The decomposition of on-site excitations according to their precise local environment offers a very useful perspective on electronic excitations in magnetic materials. Here, the comparison hints at the importance of Ni1···Ni2 interactions. In addition to providing a superb platform for the exploration of coupled charge and spin degrees of freedom, these findings reveal that the remarkable polarization properties and magnetoelectric coupling in $Ni_3TeO_6$ extend to much higher energies than previously supposed [13]. This is interesting and important because similar energy transfer processes may exist in other materials—particularly those in which transition metal centers and heavy chalcogenide cations coexist.

FIG. 4. (a),(b) Close-up view of the $^3A_{2g} \rightarrow {}^3T_{2g}$, $^3A_{2g} \rightarrow {}^1E_g$, and $^3A_{2g} \rightarrow {}^3T_{1g}$ absorption bands at 0 and 35 T along with the full field absorption difference in the $ab$ plane. (c),(d) Close-up views of the $^3A_{2g} \rightarrow {}^1T_{2g}$ excitation in the $ab$ plane and $c$ directions. The red, green, and blue hash marks indicate calculated $d$-to-$d$ excitations for Ni1, Ni2, and Ni3.

[1] D. I. Khomskii, Physics **2**, 20 (2009).

[2] F. Matsukura, Y. Tokura, and H. Ohno, Nat. Nanotechnol. **10**, 209 (2015).

[3] W. Eerenstein, N. D. Mathur, and J. F. Scott, Nature (London) **442**, 759 (2006).

[4] S.-W. Cheong and M. Mostovoy, Nat. Mater. **6**, 13 (2007).

[5] P. Chen, B. S. Holinsworth, K. R. O'Neal, T. V. Brinzari, D. Mazumdar, Y. Q. Wang, S. McGill, R. J. Cava, B. Lorenz, and J. L. Musfeldt, Phys. Rev. B **89**, 165120 (2014).

[6] H. Matsuzaki, H. Nishioka, H. Uemura, A. Sawa, S. Sota, T. Tohyama, and H. Okamoto, Phys. Rev. B **91**, 081114(R) (2015).

[7] N. Poudel, K.-C. Liang, Y.-Q. Wang, Y. Y. Sun, B. Lorenz, F. Ye, J. A. Fernandez-Baca, and C. W. Chu, Phys. Rev. B **89**, 054414 (2014).

[8] K. Taniguchi, N. Abe, T. Takenobu, Y. Iwasa, and T. Arima, Phys. Rev. Lett. **97**, 097203 (2006).

[9] O. Heyer, N. Hollmann, I. Klassen, S. Jodlauk, L. Bohaty, P. Becker, J. A. Mydosh, T. Lorenz, and D. Khomskii, J. Phys. Condens. Matter **18**, L471 (2006).

[10] F. Ye, R. S. Fishman, J. A. Fernandez-Baca, A. A. Podlesnyak, G. Ehlers, H. A. Mook, Y. Wang, B. Lorenz, and C. W. Chu, Phys. Rev. B **83**, 140401(R) (2011).

[11] T. Aoyama, K. Yamauchi, A. Iyama, S. Picozzi, K. Shimizu, and T. Kimura, Nat. Commun. **5**, 4927 (2014).

[12] I. Živković, K. Prša, O. Zaharko, and H. Berger, J. Phys. Condens. Matter **22**, 056002 (2010).

[13] Y. S. Oh, S. Artyukhin, J. J. Yang, V. Zapf, J. W. Kim, D. Vanderbilt, and S.-W. Cheong, Nat. Commun. **5**, 3201 (2014).

[14] F. Wu, E. Kan, C. Tian, and M.-H. Whangbo, Inorg. Chem. **49**, 7545 (2010).

[15] J. W. Kim, S. Artyukhin, E. D. Mun, M. Jaime, N. Harrison, A. Hansen, J. J. Yang, Y. S. Oh, D. Vanderbilt, V. S. Zapf, and S.-W. Cheong, Phys. Rev. Lett. **115**, 137201 (2015).

[16] M. O. Yokosuk, S. Artyukhin, A. al-Wahish, X. Wang, J. Wang, Z. Li, S.-W. Cheong, D. Vanderbilt, and J. L. Musfeldt, Phys. Rev. B **92**, 144305 (2015).

[17] K. Dewhurst, S. Sharma, L. Nordström, F. Cricchio, F. Bultmark, O. Grånäs, H. Gross, C. Ambrosch-Draxl, C. Persson, C. Brouder et al., The Elk FP-LAPW Code, http://elk.sourceforge.net.

[18] F. Bultmark, F. Cricchio, O. Grånäs, and L. Nordström, Phys. Rev. B **80**, 035121 (2009).

[19] V. I. Anisimov, I. V. Solovyev, M. A. Korotin, M. T. Czyżyk, and G. A. Sawatzky, Phys. Rev. B **48**, 16929 (1993).

[20] J. P. Perdew and Y. Wang, Phys. Rev. B **45**, 13244 (1992).

[21] See Supplemental Material at http://link.aps.org/supplemental/10.1103/PhysRevLett.117.147402 for more details on calculations and spectroscopic data.

[22] C. J. Ballhausen, Introducton to Ligand Field Theory (McGraw-Hill Book Co., Inc., New York, 1962).

[23] R. Eder, in Correlated Electrons: From Models to Materials Modeling and Simulation, Vol. 2, edited by E. Pavarini, E. Koch, F. Anders, and M. Jarrell, (Verlag des Forschungszentrum Jülich, Augsburg, 2012).

[24] S. L. Reddy, T. Endo, and G. S. Reddy, in Advanced Aspects of Spectroscopy, edited by M. A. Farrukh (InTech, 2012).

[25] Ni1 is strongly distorted, Ni2 is the most symmetric $C_3$ site, and Ni3 is the most distorted of all [12].

# Supplementary information for "Magnetoelectric coupling through the spin flop transition in $Ni_3TeO_6$"

M. O. Yokosuk,[1] Amal al-Wahish,[1] Sergey Artyukhin,[2] K. R. O'Neal,[1] D.

Mazumdar,[1] P. Chen,[1] Junjie Yang,[3] Yoon Seok Oh,[2,4] Stephen A. McGill,[5]

K. Haule,[2] Sang-Wook Cheong,[2,3,4] David Vanderbilt,[2] and J. L. Musfeldt[1,6]

[1] *Department of Chemistry, University of Tennessee, Knoxville, Tennessee 37996 USA*

[2] *Department of Physics and Astronomy, Rutgers University, Piscataway, New Jersey 08854, USA*

[3] *Laboratory for Pohang Emergent Materials and Max Plank POSTECH Center for Complex Phase Materials,*

*Pohang University of Science and Technology, Pohang 790-784, Korea*

[4] *Rutgers Center for Emergent Materials, Rutgers University, Piscataway, New Jersey 08854, USA*

[5] *National High Magnetic Field Laboratory, Florida State University, Tallahassee, Florida 32310, USA*

[6] *Department of Physics and Astronomy, University of Tennessee, Knoxville, Tennessee 37996 USA*

## Assignment of the $d$-to-$d$ excitations

A Tanabe-Sugano diagram provides a useful framework with which to reveal the nature of on-site $d$-to-$d$ excitation in transition metal-containing materials. The diagram for a $d^8$ electron configuration is shown in Fig. S1(a). The strength of the crystal field is, of course, given by $Dq/B$. The red vertical line indicates a best fit of the crystal field strength for $Ni_3TeO_6$. Taking a closer look, the lowest energy excitations (at that value of $Dq/B$) are expected to be $^3A_2 \rightarrow {}^3T_2$, $^3A_2 \rightarrow {}^1E$, and $^3A_2 \rightarrow {}^3T_1$. Here, $^3A_2$ is the ground state. Figure S1(b) shows a close-up view of the same diagram, rotated by $90°$ for comparison with the measured absorption spectrum of $Ni_3TeO_6$. Each excitation in the absorption matches with predicted excitations from the Tanabe-Sugano diagram. This indicates that the peaks seen the absorption spectrum of $Ni_3TeO_6$ should be assigned as on-site $d$-to-$d$ excitations. This very general framework for $Ni^{2+}$-containing materials is extended by our more detailed calculations (described below) which account for the subtly different environments of Ni1, Ni2, and Ni3.

## Calculation details

The density of states and RPA susceptibility were calculated using the Elk code and LDA+U approximation with $U = 4$ eV on Ni $d$ orbitals. In order to estimate the $d$-to-$d$ transition energies we have used the Wien2K-DMFT code by Kristjan Haule to calculate the Wannier functions within the energy window spanning only the $3d$ Ni orbitals. The dynamic crystal field produced by oxygens in DMFT is then replaced by the static crystal field, encoded in the Wannier orbital energies. The on-site Hamiltonians (using $J_H = 0.9$ eV) in the basis of these Wannier functions were diagonalized independently for the three Ni sites and the distances
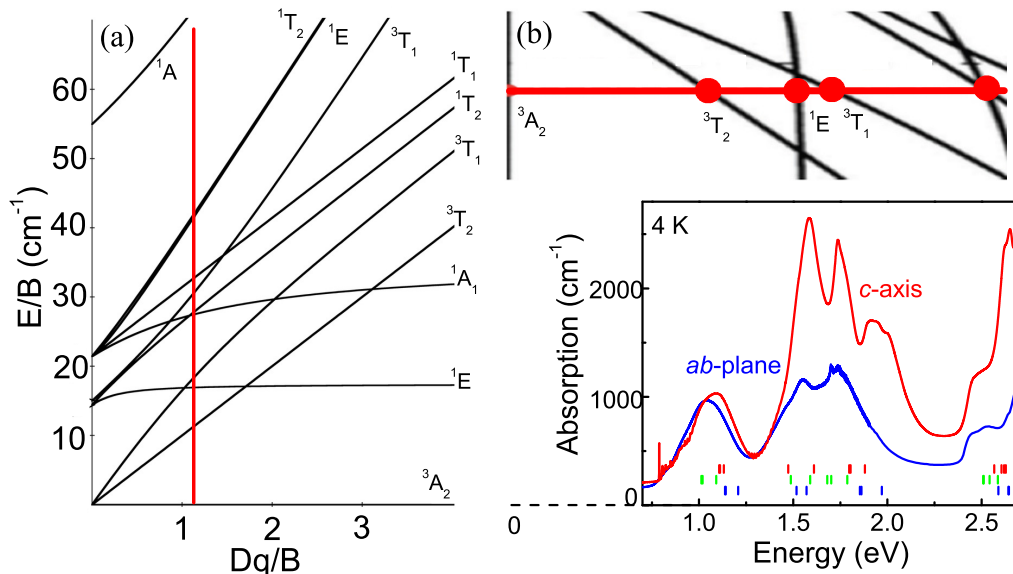
FIG. S1: (a) Tanabe-Sugano diagram for a $Ni^{2+}$ center in the $d^8$ configuration. The crystal field strength of $Ni_3TeO_6$ is shown in red. (b) Here, the Tanabe-Sugano diagram is turned on its side and paired with the absorption spectrum along the $ab$-plane and $c$-axis. The calculated Ni $d$-to-$d$ excitations for each of the three distinct Ni centers are displayed as red, green, and blue hash marks. Expectations from the Tanabe-Sugano diagram and the theoretically predicted excitations align very well with our experimental observations.

between the ground and excited states were used to approximate the $d$-to-$d$ transition energies. These energies are marked by red, green, and blue vertical bands in Fig. S1(b). The calculated excitations for Ni1, Ni2, and Ni3 group into band clusters that are located in the general vicinity of the $d$-to-$d$ transitions identified from the much simpler Tanabe-Sugano model discussed above.

FIG. S2: (Color online) Results of DFT calculations on $Ni_3TeO_6$: (a) ion-projected density of states per magnetic unit cell, (b) splitting of free Ni ion $d^8$ multiplets in the presence of an octahedral crystal field and the crystal field excitations between these levels, and (c) components of linear optical dielectric response tensor calculated within the random phase approximation in the $q \to 0$ limit with no microscopic contributions (solid lines: with spin-orbit coupling included; dashed: without).
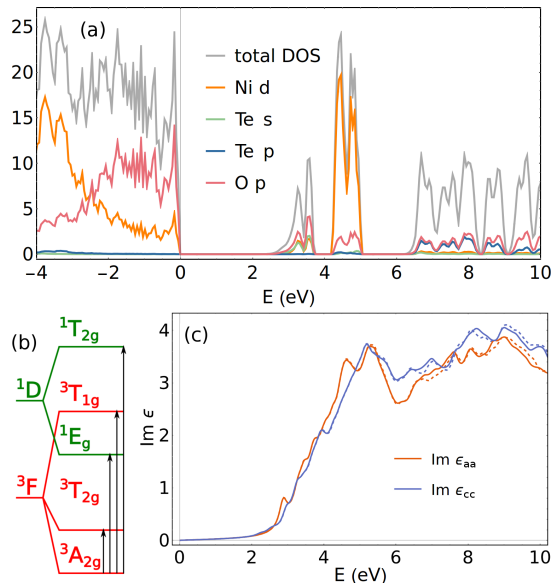
## Temperature dependence around the magnetic transition

Along with the field induced changes across the spin flop transition, we also tested whether the electronic properties of $Ni_3TeO_6$ were sensitive to the 53 K magnetic ordering transition. Figure S3 shows absorption difference spectra as a function of temperature at fixed field. No distinctive changes are observed across the Neél transition. In other words, the temperature dependence in this range is very systematic.
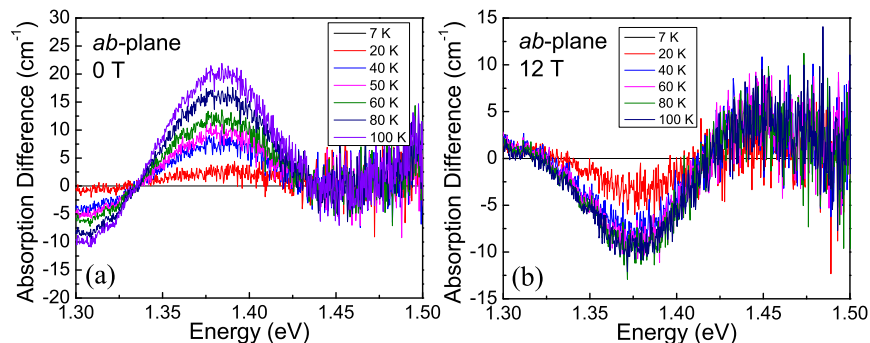


FIG. S3: Variable temperature absorption difference, $\Delta\alpha = [\alpha(E, T) - \alpha(E, T = 7\text{ K})]$, at (a) 0 T and (b) 12 T.

## Absolute absorptions in high magnetic field

Figure S4 shows the absorption spectra of $Ni_3TeO_6$ in the *ab*-plane and along *c* at 0 and 35 T. The full field data was back-calculated by adding the absorption difference curve at 35 T (calculated as $\Delta\alpha = \alpha(E, B = 35\ T) - \alpha(E, B = 0\ T)$) to the spectrum taken at 0 T. As in the main text, the absorption difference spectrum is plotted for comparison. Because the three Ni ions have different local environments (and therefore different crystal field splittings), each set of Ni *d*-to-*d* excitation energies is distinct. Since the Ni3 environment is most distorted from a perfect octahedral environment, it has the largest crystal field splitting, and the predicted excitations emanating from these sites have the overall highest energies. By contrast, the Ni2 centers have the least distortion, the smallest crystal field splitting, and the overall lowest energies within each cluster of excitations. This is equivalent to moving left and right along the $Dq/B$ axis of Fig. S4(a).

It's easy to see from Fig. S4 that the optical properties of $Ni_3TeO_6$ change with applied field. A closer view is, however, required to link these modifications with distortions and the associated crystal field splittings around each of the Ni centers. For comparison, each cluster of excitations (both predicted and measured) is shown separately in Figs. S5 and S6. While some energy windows are more revealing than others, several general trends emerge.

For instance, in the majority of cases, the leading edge of the band (and sometimes other energy windows near the center) are affected by magnetic field. This suggests that the local environment around Ni2 (and probably Ni1 as well) becomes more distorted, although probably still remaining within the same point group. By contrast, the trailing edge of each of the bands has very limited or no field dependence. Since
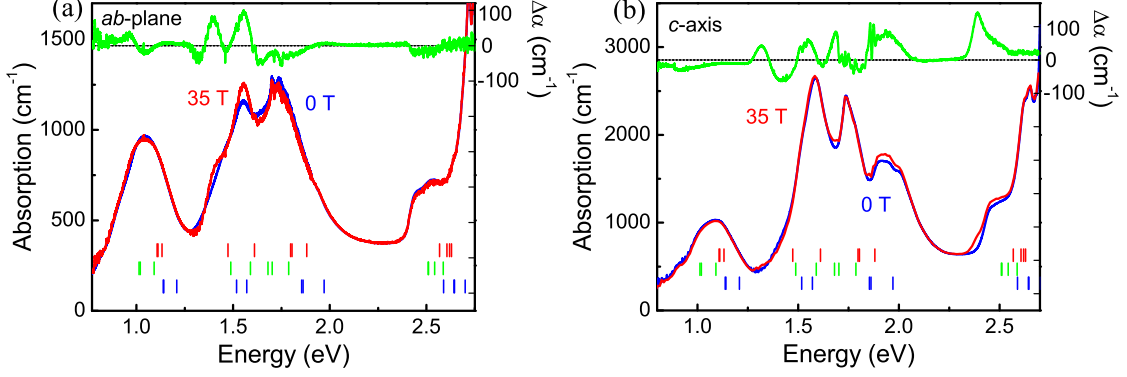
FIG. S4: (a) Absolute absorption spectrum of $Ni_3TeO_6$ at 0 and 35 T in the $ab$-plane along with the full field absorption difference at 4.2 K. (b) Absorption spectrum at 0 and 35 T in the $c$-direction along with the absorption difference given by $\Delta\alpha = \alpha(E, B = 35\ T) - \alpha(E, B = 0\ T)$ at 4.2 K. The vertical tick marks at the bottom of each graph indicate the predicted $d$-to-$d$ excitation energies of each of the Ni centers (Ni1 in red, Ni2 in green, Ni3 in blue).
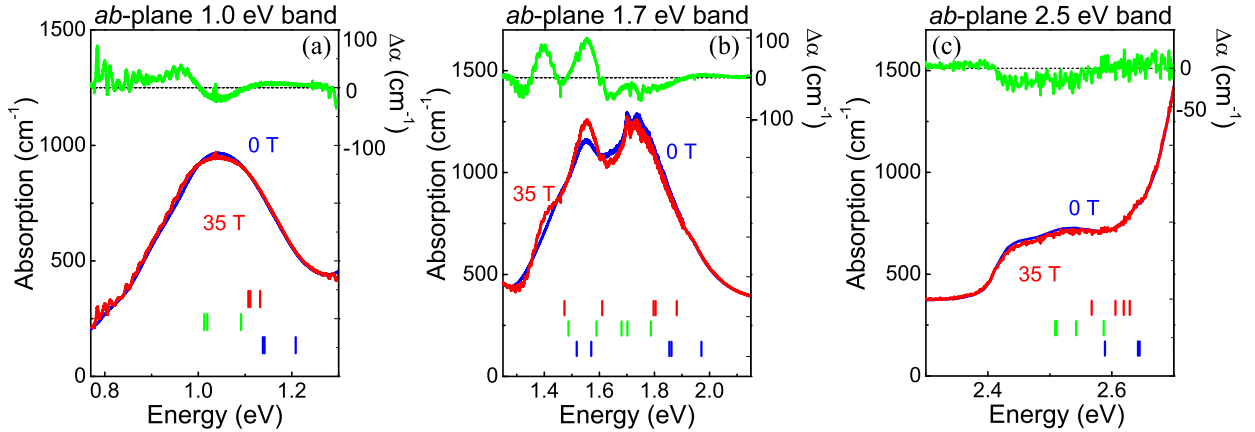


FIG. S5: Close-up views of the Ni $d$-to-$d$ excitations in the vicinity of the (a) 1.0, (b) 1.7, and (c) 2.5 eV bands in the $ab$-plane. The set of vertical tick marks show the calculated excitations for each type of Ni center (Ni1 in red, Ni2 in green, Ni3 in blue). As discussed here and in the main text, the relative position of these excitations reveals the relative size of the crystal field splitting.

we know (based upon the predicted sequence of excitations) that the $d$-to-$d$ excitations emanating from the Ni3 centers always govern the shape of the band tail, we surmise that the local structure around the Ni3 centers is not very sensitive to magnetic field. This is probably because the Ni3 site is already strongly distorted, allowing this metal center and the ligands around it to remain rigid under applied field. These findings are in excellent agreement with the predictions of Wu $et\ al.$ on the importance of superexchange within the Ni1···Ni2 pair to the magnetic properties [S1].
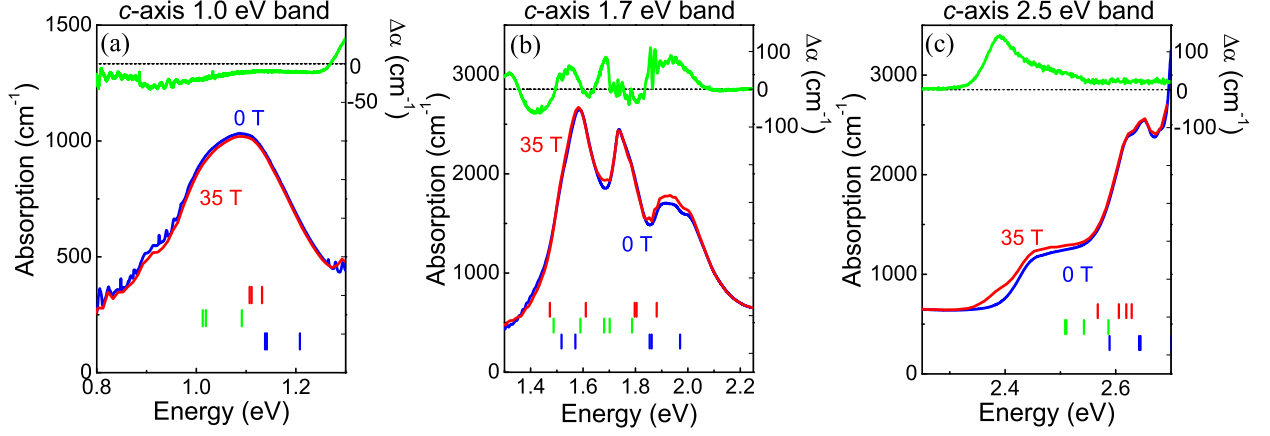
FIG. S6: Close-up views of the Ni $d$-to-$d$ excitations in the vicinity of the (a) 1.0, (b) 1.7, and (c) 2.5 eV bands in the $c$-direction. The set of vertical tick marks at the bottom of each panel indicate the calculated excitations for each type of Ni center (Ni1 in red, Ni2 in green, Ni3 in blue) [S2].

## Trends in the integrated absorption difference

The fundamental electronic excitations of $Ni_3TeO_6$ display a number of different trends across the 9 T spin flop transition. These are best seen in the absorption difference, $\Delta\alpha(E, B) = \alpha(E, B) - \alpha(E, B = 0)$, which eliminates spectral commonalities. In a complex spectrum, it is challenging to fully disentangle energy, linewidth, and oscillator strength trends. $Ni3TeO_6$ is even worse than usual because there are three different Ni centers. This means that the band centered at 1.0 eV has 9 different oscillators! And the bands centered near 1.7 eV have a total of 15 underlying $d$-to-$d$ excitations - each with their own oscillator parameters! So while we examined the lineshapes carefully to see whether specific energy, linewidth, and oscillator strength trends could be unraveled, there are no unambiguous trends. We therefore elected to employ an integral of the absolute value of the absorption difference $\int(\Delta\alpha)dE$ over an appropriate energy window to track what is actually a combination of energy, linewidth, and oscillator strength changes for 9 or 15 individual oscillators. Examples of these trends, which are responsive to the static structural environment, are shown in Fig. S7. Sharp changes are observed across the spin flop transition, irrespective of the energy window in which the magneto-optical properties are analyzed. That said, oscillator strength changes can increase or decrease and even (in the case of the response centered around 1.4 eV) give an indication of the higher field transitions to come. These interesting differences may contain clues to the complex interplay of competing interactions in this material.
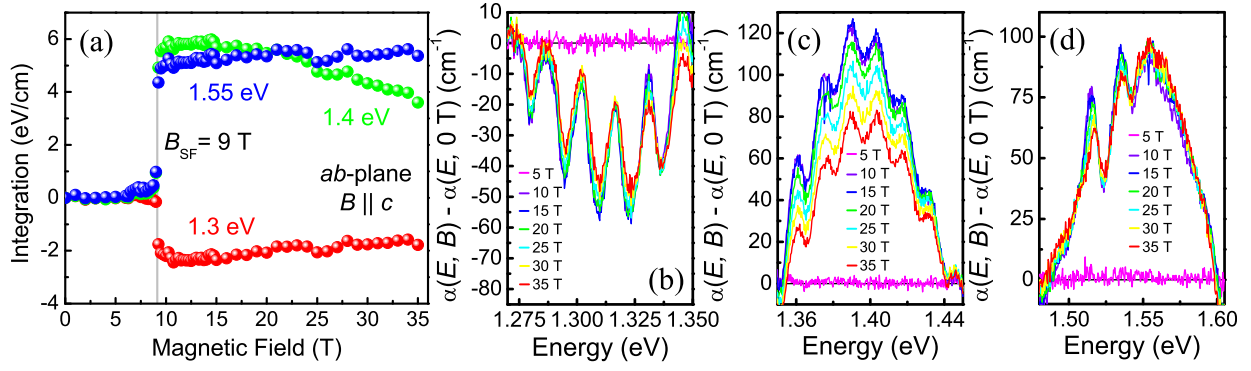
FIG. S7: (a) Integrated absorption difference vs. magnetic field in several different energy windows in the *ab*-plane. The red points correspond to analysis of the spectral data in panel (b), the green points with (c), and the blue with data in (d). The 9 T spin-flop transition is indicated by a vertical gray line.

---

[S1]  F. Wu, E. Kan, C. Tian, and M. -H. Whangbo, Inorg. Chem. **49**, 7545 (2010).

[S2]  Additional resolution is required to track changes in the exciton and phonon sidebands in applied field.